WDS'05 Proceedings of Contributed Papers, Part II, 285–294, 2005. *ISBN 80-86732-59-2* © *MATFYZPRESS*

A Model of Secondary Emission and Its Application on the Charging of Dust Grains

I. Richterová, J. Pavlů, Z. Němeček, and J. Šafránková

Charles University, Faculty of Mathematics and Physics, Prague, Czech Republic.

Abstract. Dust grains of various shapes and materials can be found anywhere in the space where the temperature decreases under a melting point. Many plasma processes are driven by the grain charge but, on the other hand, dust grain charging can be influenced by several different processes, too. Among others, secondary emission can play a dominant role wherever the plasma is hot.

In the present paper, a further development of our previous simple numerical secondary emission model, now using techniques for a beam interaction modelling applied in electron microscopies, is sketched and its application onto charging of spherical dust grains by a narrow electron beam is discussed. The model fits experimental data rather well and, thus, our conclusion suggests that the model is a very useful tool for considerations on the dust charging under different conditions in the space.

Introduction

It is widely known that particulate matter with a size distribution from micro to nanometres (dust) is a substantial part of the interstellar medium as well as of different laboratory environments. Immersed in a plasma, the dust is charged by various processes and finally reaches an equilibrium state. The most important processes leading to dust charging range from the attachments of ions and electrons of the ambient plasma to all kind of emissions (induced by the UV radiation, particle impacts, or a strong electric field) [*Whipple*, 1981]. Dust grains charge typically negatively in the space plasma, however, secondary electron emission may lead to a positive dust charge when the high-energy electron fluxes dominate, e.g., in planetary magnetospheres [*Kimura and Mann*, 1998]. The composition of dust grains in plasmas can be diverse and many materials have a secondary emission yield larger than unity [*Horányi*, 1996]. It is generally expected that the secondary emission yield is related to surface properties of the bombarded body. Nevertheless, secondary emission from small bodies is determined not only by their composition but an effect of their dimensions becomes very important when the penetration depth of primary electrons is comparable to the grain size. On the contrary to well-described emission properties of large planar samples [e.g., *Sternglass*, 1951], corresponding characteristics of the dust grains are accounted very approximately [*Draine and Salpeter*, 1979].

The knowledge of dust grain emission yields seems to be central in dusty plasma dynamics for providing also information of plasma particle energy distribution changes caused by emissions. There are several spacecrafts (e.g., Stardust or Cassini) detecting *in-situ* dust grain features (their charge, mass, size, and composition). Nevertheless, observing particular charging processes separately is impossible this way because experimental conditions are not too adjustable. A simplest way to study a secondary electron emission from dust consists in measuring an equilibrium charge of spherical grains affected by a mono-energetic beam and several such laboratory experiments had been performed. *Švestka et al.* [1993] found the second growth of an equilibrium grain surface potential above about 10 keV for a 2.2 μm glass grain but they had some troubles with background currents that make the results a bit uncertain. Other measurements were done with submicron oil and micron metal grains by *Ziemann et al.* [1995] and *Velyhan et al.* [2001], respectively. However, they dealt with lower beam energy ranges and, thus, the second potential growth was not observed.

We had developed a simple Monte Carlo model of secondary emission from spherical dust grains and its results had been confirmed by calculating the consequent equilibrium grain potential [*Richterová et al.*, 2004]. The model could be also applied on a planar geometry what allows us to compare computed yields with an extensive set of experimental data [e.g., *Bronstein and Fraiman*, 1969]. Although our model provides a typical secondary yield curve and can roughly describe observed energetic dependences of a dust grain equilibrium charge, it has numerous non-measurable parameters. Further, neither a backscatter yield matches the experimental data very well nor depends on a sample material in the model. Nevertheless, it was shown that the increase of a dust grain equilibrium charge at a high-

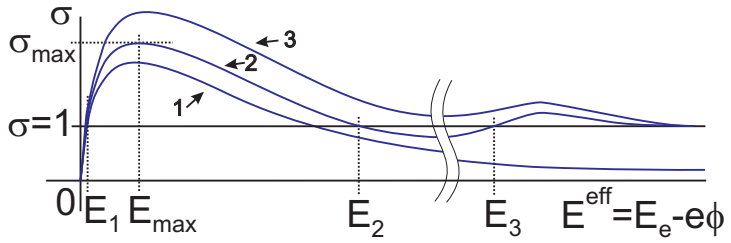

Figure 1. Schematics of the total secondary yield dependence on an effective beam energy: (1) a large planar surface, (2) a dust grain from the same material, and (3) another dust grain with a higher value of the SE yield maximum. The SE yield enhancement leads to positive equilibrium potentials for high energies. Note that for very high energies σ approaches η which is equal unity for dust grains as no PE can be calmed down in such a tiny piece of matter.

energy beam range should be attributed to enhancement of a yield of scattered electrons rather than that of secondary electrons as suggested by *Chow et al.* [1994]. To receive a better approximation of the backscatter yield, the model have been amended by assumptions of a primary electron behaviour closer to a physical description of electron—solid interaction using a technique known in a low-energy beam Monte Carlo modelling for a scanning electron microscopy [*Joy*, 1995]. In this paper, the theoretical background and assumptions of the new model and comparison of modelled and measured data on large planar as well as small spherical samples consist of single chemical elements or glass are presented.

The testing measurements have been performed using apparatus described by *Čermák et al.* [2004]. The experiment is based on a detection of a single dust grain motion inside a 3D electrodynamic trap (*a Paul trap*) where the levitated grain oscillates. The only quantity of a trapped grain which our experimental set-up allows us to measure is its oscillation frequency or, in other words, the grain specific charge (charge-to-mass ratio, Q/m). Other characteristics like a grain surface potential or charging currents can be also evaluated. Our realisation of a Paul trap limits our measuring range from $\approx 10^{-3}$ to 40 C/kg. The experimental equipment is complemented with an electron ($\approx$ 100 eV $\div$ 10 keV) gun. The whole set-up is kept under ultra-high vacuum (typically better than 10^{-6} Pa) to suppress any possible effect caused by the grain and beam interactions with the residual atmosphere. For a comparison of model results with laboratory simulations, we have chosen spherical gold (diameters 0.6–2 μm) and glass (diameter 1.2 μm) grains.

Electron — solid interaction

Primary electrons (PEs) impacting the sample surface interact with a bulk material. They lose their energy in many types of collisions what often results in excitations of material electrons. Some of the excited electrons can then leave the surface. These electrons, so-called true secondary electrons (SEs), have typically energies of a few eV (with a Maxwellian-like energy distribution). For large planar samples, the energetic dependence of the secondary emission yield (defined as a mean number of secondaries per one PE), δ, can be described by the Sternglass' universal curve [*Sternglass*, 1951]. This curve exhibits a maximum at a few tenths of keV and decreases to zero at very high and low beam energies. Its parameters, the maximum yield, δ_{max}, and the corresponding energy, E_{max}, depend only on a sample material at a certain incident angle. During collisions, PEs change their direction and thus may be backscattered (BEs) from the material before losing all of their energy. Their yield, η, increases with a material density and an atomic number up to ≈ 0.5 for a normal incident angle. It grows only slowly with a beam energy above a few hundreds of eV. Thus, both the total secondary yield, $\sigma = \delta + \eta$, and δ vary in a similar way with the beam energy [*Bronstein and Fraiman*, 1969].

Whereas both yields can be measured directly for large samples, in the case of an isolated dust grain, only the equilibrium surface potential can be obtained readily. Currents flowing from/to the grain are related to the grain potential and vice versa. The equilibrium grain surface potential, ϕ, is reached when the net current is zero. The surface potential depends on grain material, size, and shape, on surrounding plasma parameters, and on a charging history [*Meyer-Vernet*, 1982].

An attachment of PEs is accompanied with an emission of SEs and BEs at any energy. For a narrow electron beam, the equilibrium grain surface potential is determined by secondary electron emission until being high enough for other inseparable processes like ion and electron field emissions, electrostatic fragmentation, etc. The grain is charged positively only if σ exceeds unity. If we use the quantity σ exactly in accordance with its definition — i.e., as a ratio of corresponding currents, it would mean that

this quantity, σ_ϕ depends not only on the material, energy, and angle of incident electrons but it is also a function of ϕ. Since most of SEs have energies of a few eV, σ_ϕ then decreases rapidly with ϕ as they are unable to escape from a charged grain and thus the equilibrium potential (given now by $\sigma_\phi = 1$) cannot exceed a few volts. On the other hand, scattered electrons have much higher energies than secondaries and can always leave the grain and thus do not deposit their charge in it. As a consequence, ϕ is a function of $\delta^* = \delta/(1-\eta)$ which is determined just by a profile of SE spectrum[1].

The energy dependence of a total secondary yield for grains does not fully follow the universal curve for large samples. First, it is enhanced due to a surface curvature that results in a variation of an incident angle along the grain surface[2]. (For grain potential of a few eV, σ changes caused by a beam deflection (i.e., secondary incident angle variation) can be neglected.) Second, when the penetration depth of PEs is comparable with a grain size the PEs become able to leave the grain more often and thus, the total secondary yield grows again and can be greater than unity for a high-energy beam. An energy dependence of σ and its variation with a sample shape is sketched in Fig. 1.

Our model — assumptions and results

A few attempts of modelling of a δ enhancement and a corresponding surface potential for dust grains were made [e.g., *Draine and Salpeter*, 1979; *Chow et al.*, 1994; *Ziemann et al.*, 1995] but these models did not match observed behaviour very well at a high-energy range. *Ziemann et al.* [1995] did not consider their model for beam energies associated with a beam penetration through grains at all. *Draine and Salpeter* [1979] estimated the δ enhancement due to a grain shape and size but he did not take into account an energy distribution of emitted electrons. *Chow et al.* [1994] made a precise analytical model following in basic secondary emission theories. Nevertheless, they did not regard any beam scattering inside a grain what caused rapid second potential growth when a beam penetration depth is nearly equal to the grain size. Moreover, a resulting yield curve profile (need be integrated numerically) was quite sensitive on chosen integrating method. One would expect that beam scattering inside a grain could clarify the nature of observed dependences.

For a better description of a dust grain response to hot electron impacts, we have developed a numerical Monte Carlo model which is based on monitoring of each PE inside the sample. This approach allows us to obtain directly the BE yield. Generally, each electron suffered a specific sequence of scattering events (both elastic and inelastic) all of which can be hardly taken into account exactly (mostly because of the complexity of such processes). Therefore, several simplifications are needed. In the earlier version of our model [*Richterová et al.*, 2004], especially a contribution of a beam scattering inside the matter

[1]This statement can be found as follows: $\sigma_\phi = \sigma \int_{e\phi}^{\infty} F_{AE}dE = \delta \int_{e\phi}^{E_0} F_{SE}dE + \eta \int_{E_0}^{\infty} F_{BE}dE = \delta \int_{e\phi}^{E_0} F_{SE}dE + \eta = 1$, where $F_{AE}, F_{SE}, \text{and} F_{BE}$ are distribution functions of all emitted, secondary, and backscattered electrons, respectively, and E_0 is the commonly defined separator being of about 50 eV. Note that $e\phi$ is always less than E_0 in this simplification until η itself is supposed to be less than unity.

[2]For planar samples, σ (and both constituents, δ as well as η) increases with an incident angle [*Bronstein and Fraiman*, 1969].

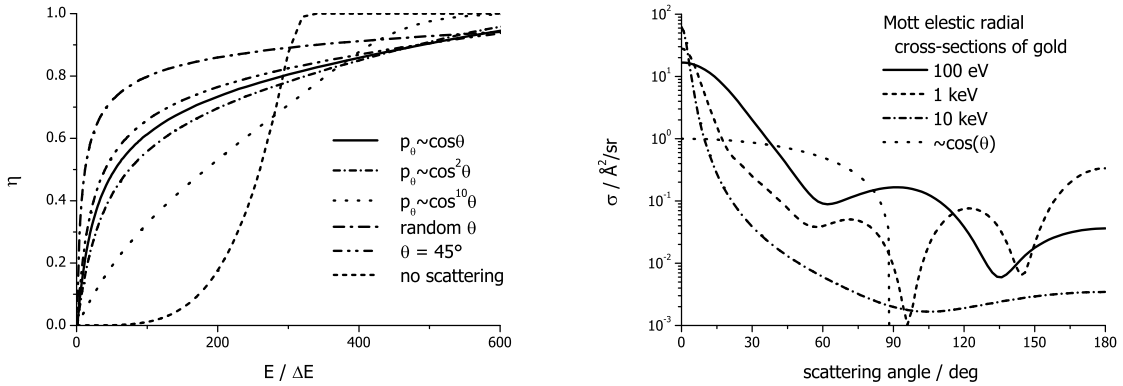

Figure 2. A BE yield as a function of an energy for different deflection distributions at a collision ($\Delta E \approx 35$ eV) (left) and comparison of Mott elastic radial scattering cross-sections of gold [*Mott and Massey*, 1965; *Czyżewski et al.*, 1990] to the cosine distribution (right). The main difference between models is an angular cross-section dependence.

onto secondary emission yields had been studied. We started with rather rough approximations aimed especially for model clarity and numerical easiness. The assumptions that had been chosen were as it follows:

(1) Samples consist of a continuous and homogenous matter[3] characterised by a few material constants. No detailed real atomic or electronic structures are considered.

(2) A PE moves along a straight line between collisions.
   – In each collision, a constant amount of an energy, ΔE, is spent and the PE direction is altered according to a simple distribution such like a cosine law (independently on the PE energy).
   – A mean free path of PEs decreased linearly with the lost energy.

(3) One material electron is excited during each collision and then it behaves independently on the PE.

(4) A probability, P, that excited material electrons reach the surface decreases exponentially with the distance to it, x, $P \sim \exp(-x/\Lambda)$. The mean free diffusion path of secondaries, Λ, is expected to be of the order of a lattice constant for metals and much longer for insulators [*Sternglass*, 1951].

(5) For an equilibrium grain potential modelling, the SE energy spectrum profile[4] must be employed. A random energy in accordance with a chosen distribution is generated for each SE and it escapes from the grain when this energy is larger than the actual grain potential.

Although the model provided relevant δ curve, as a consequence of the second assumption, a number of BEs remained independent on material and, moreover, exceeded significantly experimental values. Fig. 2 (left) shows that the number of BEs cannot be pronouncedly changed using different distributions of the scattering angle, θ. Nevertheless, the grain potential growth at the high-energy beam range was predicted. It was shown that this growth is caused by the η enhancement and not by the δ increase when a penetration depth of PEs becomes comparable with a grain size. Therefore modelled values of η matching better real observations are needed and, in this case, the model was improved applying energy and material dependent cross-sections known in a beam interaction modelling used in electron microscopies [*Joy*, 1995]. In the new model, the assumptions (1), (4), and (5) are held, (2) and(3) are changed in the following way:

(2) For description of PEs trajectories inside the matter, a single scattering model according to *Hovington et al.* [1997] is used:
   – a PE moves along straight lines between collisions. Above about a few tenths of keV, almost all non-negligible deflections are caused just by elastic electron-atom collisions [*Egerton*, 1986]. Thus, Mott radial elastic cross-sections [*Mott and Massey*, 1965] namely values computed by *Czyżewski et al.* [1990][5] are employed. As an example, the Mott radial elastic scattering cross-sections at several energies is given for gold in Fig. 2 (right). Their advantages (instead of any approximative function usually used [*Joy*, 1995]) are especially a better accuracy as well as shorter computation times.
   – all possible energy losses are averaged and thus each PE loses the energy continuously along its path (the modified Bethe stopping power equation[6] is used).

For keeping the model integrity, assumption (3) is varied to:

(3) Whole deposited energy is converted to electron excitations, only. A number of excited electrons is related to the energy spent by the mean excitation energy, ε. Excited material electrons behave independently on the collision type and/or on the PE energy or direction.

The principles of the new model are illustrated in Fig. 3.

Only three free parameters — ε, Λ, and a SE spectrum — remain in our model and their influence on the model results will be examined in several following figures. A dependence of a modelled SE yield maximum on a mean free diffusion path of secondaries is shown in Fig. 4 (left) for several materials. All

[3]This also means that grains are big enough. The model cannot be valid for, e.g., small atomical/molecular clusters often present in the space.

[4]According to the third assumption, we suppose that this spectrum does not vary with the beam energy.

[5]The computations were made for several energies between 20 eV and 30 keV, only. In this energy range, any required value is then obtained by a cubic spline interpolation.

[6]The modified Bethe stopping power equation can be written as $\frac{dE}{ds} \sim \rho \frac{Z}{AE} \ln(\frac{1.166E}{J})$ where ρ is the sample mass density, Z and A are the atomic and neutron numbers, respectively, J is close to the mean ionisation potential, ds is the path element, and E is the actual electron energy [*Hovington et al.*, 1997].

curves exhibit similar profiles, i.e., δ_{max} are roughly a power function of Λ^{-1} for planar as well as for spherical samples. $\varepsilon\delta_{max}$ increases with the atomic number at certain Λ except of a very small Λ where the model validity terminates. The increase corresponds to a greater amount of a deposited beam energy nearer to a sample surface as the beam is more effective slowed down in higher atomic number materials. δ_{max} for grains may be as much as several times larger than for planar samples, however, the difference disappears at higher Λ. $\varepsilon\delta_{max}$ is plotted as a function of E_{max} for the same samples in Fig. 4 (right). The dependences were obtained varying Λ as those in the left figure and a linear relation was found. Since the E_{max} values were mechanically taken from modelled curves which are noisy and exhibit rather flat maxima, some inaccuracy may occur and the waving of several curves is due to it.

Our model provides also a great amount of detailed data such a distribution of beam energy losses in the sample or BE spectra. A concise analysis of them was performed for a gold planar sample at a beam energy range from 50 eV to 15 keV and a normal incident angle as a demonstration of the model potentiality. BE spectra for several beam energies are plotted in Fig. 5 (left). All of them have a typical profile with the maxima close to an initial beam energy above 500 eV. A ratio of low-energy scattered electrons decreases with the beam energy and profiles of the curve maximum become rather flat for highest energies. A mean energy of scattered electrons (Fig. 5 (right)) was found to be a linear function of a beam energy or, in other words, since η is roughly constant above 1 keV, scattered electrons carry out of the grain a constant portion of the initial beam energy. Summing all energy losses of PEs at each coordinate, the distribution of beam energy losses in the sample can be obtain. Such data for several energies are plotted in Fig. 6 (left) as a function of a distance to the sample surface. A logarithmic scale has been chosen in order to show all curves in one figure. However, we can note that they are nearly symmetric around their maxima when plotted in a linear scale. *Sternglass* [1951] made a precise study on a secondary emission process that led to a similar curve shape. On contrary to many other authors, he supposed that the beam scattering is fundamental for the process understanding. He also assumed that a non-negligible part of PEs undergoes collisions which lead to a serious energy losses like, e.g., production of UV photons or Auger electrons. The re-absorbtion of these particles arises in a narrow peak of the distribution of beam energy losses close to the surface, and a peak position varies as a square root of an initial beam energy. Our model results in wider peaks and their position (Fig. 6 (right)) exhibits rather three-half power dependence. One might conclude that our assumptions are still quite simplifying to localise the origin of secondaries and a more complex model should be done. On the other hand, not all cross-sections are still known with a sufficient accuracy and our choice of model assumptions leads to adequate predictions as will be shown in the next section.

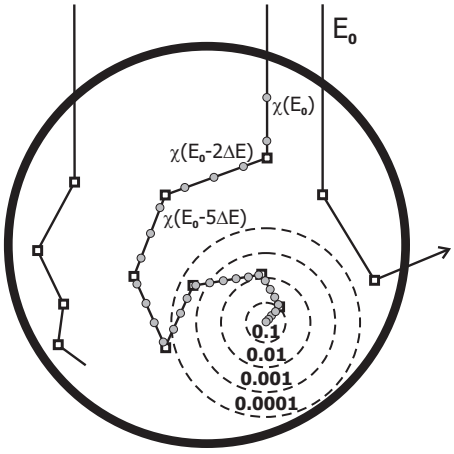

Figure 3. A 2D demonstration of our current model — visualised trajectories of PEs. PEs move straight in the matter and are scattered in collisions (marked by squares) according to Mott elastic scattering cross-sections and their actual energy. Some of them are stopped in the grain, while the others leave it. Continuous energy losing given by the Bethe stopping power formula is realised by small discrete energy losses, $\Delta\varepsilon$ along the path (marked by circles). Material electrons are excited at these coordinates with a probability $\Delta\varepsilon/\varepsilon$ and the probability that they reach the surface decreases exponentially with the distance (demonstrated only once).

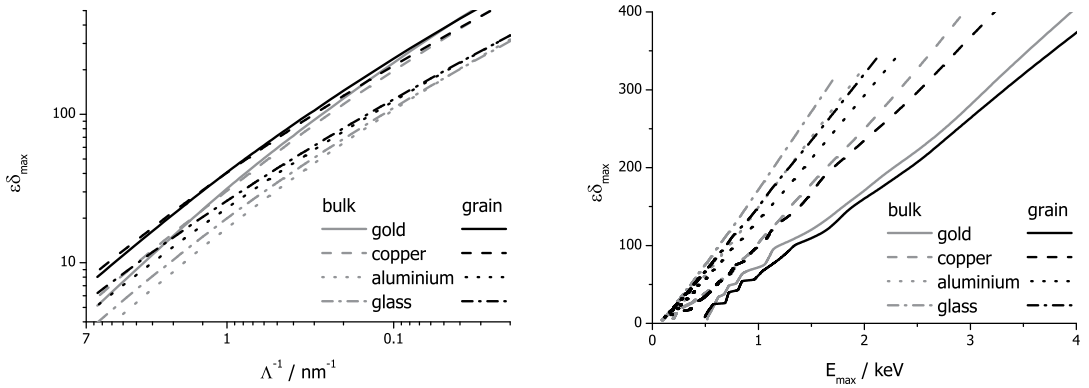

Figure 4. A modelled dependence of a SE yield maximum on the mean free diffusion path of secondaries (left) and on the energy corresponding to the maximum (right) for several materials. Planar samples and 10 cm grains are used. Note that δ_{max} is plotted in ε units. Some curves are coarse due to an error caused by a procedure of establishing of the maxima.

Comparison of the model with experimental data and its discussion

A modelled BE yield for planar samples at a normal incident angle is plotted in Fig. 7 (left) for several materials. The agreement with experimental data [*Bronstein and Fraiman*, 1969] is excellent for elements with the highest atomic numbers but a bit underestimated for the others. Also the yield maxima are a little sharper than those measured. Both differences can be caused by an increase of an inelastic collision contribution to a beam scattering since the mean ionisation potential decreases with the atomic number. Corresponding improvement of Mott elastic scattering cross-sections should be found. A local maximum under 100 eV is due to a forced interruption of a computation at the electron energy of 20 eV as the model assumptions become invalid at very low beam energies. A modelled BE yield for glass exhibits more pronounced disagreement with experimental data. It is given by two facts. First, using the Bethe stopping power equation for compounds demands an estimation of the effective mean ionisation potential what is a quite rough approach to the material structure and composition. Nevertheless, *Hovington et al.* [1997] suggested to compute the stopping power from optical absorption measurements and they obtained even better results for elements with this approach. Second, there is a lack of experimental data for a BE yield of glass and, moreover, these values vary in a broad range. This is caused also due to a fact that the scattering process and thus η are also heavily influenced by numerous admixtures often contained in glasses [*Verma*, 1977].

A comparison of a modelled SE yield with a universal curve [*Draine and Salpeter*, 1979][7] for gold

[7]This universal curve is an experimental extrapolation of the aforesaid curve found by *Sternglass* [1951] which is valid below $\approx 4E_{max}$, only.

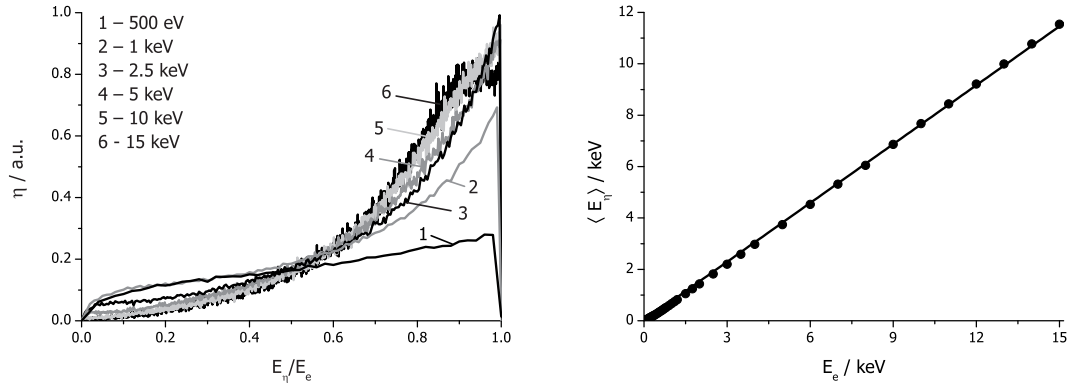

Figure 5. Left: Relative modelled spectra of scattered electrons for a planar sample. Note that the noise results from a statistic error which decreases with a number of PEs, N, as $1/\sqrt{N}$ ($N = 10^7$ used here). Right: A mean energy of scattered electrons (obtained from data similar to that presented in the left figure) as a function of a beam energy. The linear fit slope was determined to be 0.76.

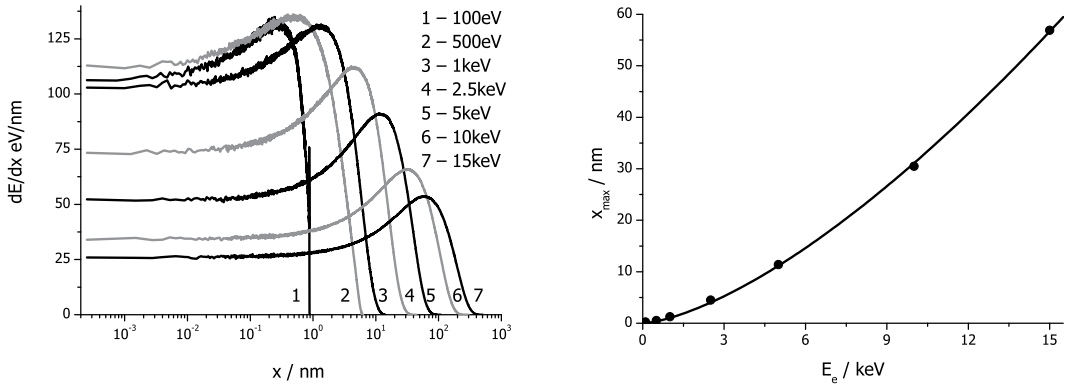

Figure 6. A modelled amount of a lost beam energy as a function of depth in a planar sample (left) and its maxima position as a function of a beam energy (right). As for the noise, see the note in Fig. 5. The fit equation is $x_{max} = 1.0{E_e}^{3/2}$ (in plot units).

is shown in Fig. 7 (right). Although they have a similar shape, our model predicts a little larger values at higher beam energies. It can be explained considering that a part of the beam energy is spent on the X-ray production. Its neglecting would result into ε overestimation ($\varepsilon = \varepsilon_{\mathrm{SE}} + \varepsilon_{\mathrm{XUV}}$), only, if it did not depend on an energy. However, the X-ray production increases with a beam energy what leads to ε growth or, in other words, in larger values of δ at higher beam energies in the case of its omission. Model results for gold grains of different diameters are also shown in Fig. 7 (right). δ_{max} and E_{max} rose about 30 % and a curve shape remained almost the same as a planar sample. A slight dependence on a diameter was found for grains smaller than ≈0.5 μm.

Measured values of an equilibrium surface potential for glass and gold grains are presented in Fig. 8. The surface potential grows with a beam energy for all grains and has a maximum at about 400 eV and 1.2 keV for glass and gold, respectively. We would like to point out that the first maximum corresponds to the δ^* yield maximum and is given by the grain material. For a glass grain, the potential increases again above about 6 keV and the growth becomes rapid at about 9 keV. For gold grains at higher beam energies, the potential only slowly decreases in an investigated energy range. Nevertheless, the decrease is less pronounced for smaller grains and one could expect its second growth for smaller diameters or at energies above 10 keV. Unfortunately, both conditions are out of our experimental possibilities. Note that the second potential growth occurs for gold grains at higher beam energies than that for the glass grain. It is due to a beam penetration depth that is shorter in gold since it is denser and has the much larger atomic number (i.e., cross-sections of PEs).

An exact equilibrium potential curve shape is driven by a SE energy spectrum and a profile of $\delta^*(E_e)$. The uncertainty of the former makes fitting to experimental data difficult. It might be therefore best to analyse the modelled yield curves first. As it was demonstrated above, the SE yield almost does

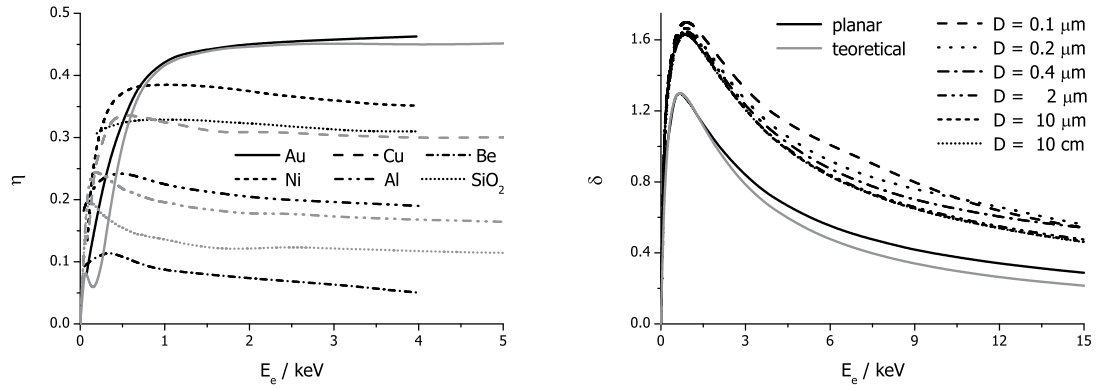

Figure 7. Left: An example of experimental [*Bronstein and Fraiman*, 1969] (black) and modelled (grey) BE yield curves for several bulk materials at a normal incident angle. η almost does not change above a few keV. Right: A modelled SE yield for gold planar sample and grains of different diameters. δ depends on a diameter for grains smaller than ≈ 0.5 μm only. The *Draine and Salpeter* [1979] universal curve is used.

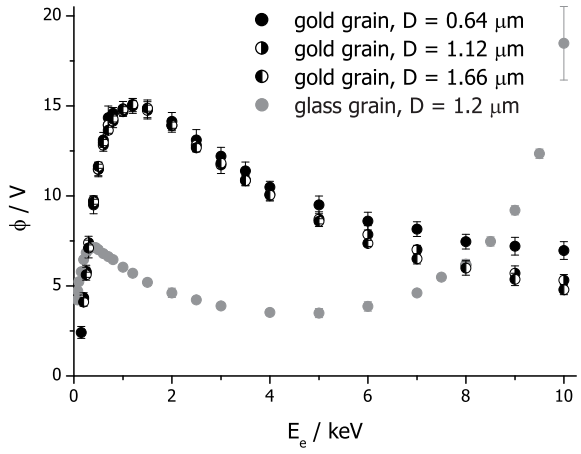

Figure 8. Experimental equilibrium characteristics of the secondary electron emission for a spherical glass grain and spherical gold grains of different diameters. The position of the first maximum is driven by surface emission properties. On the other hand, the increase of a potential at high beam energies is dominantly determined by a grain size – it needs to be comparable to a beam penetration depth.

not change across grain diameters of our interest and thus, the number of BEs remains to be a source of the second potential growth. The modelled $\eta(E_e)$ for several diameters of gold and glass grains are plotted in Fig. 9. The model results in the η enlargement under ≈ 2 μm of a grain size for gold (right part) at a given energy range. Particular curves become to differ at $\approx$ 2–3 keV for 0.6–2 μm grains what is in an excellent agreement with measured data (Fig. 8). The model also predicts an observable second potential growth at the used beam energy range for gold grains smaller than 0.5 μm. The differing point of η curves (Fig. 9 (left)) was found at $\approx$ 1–2 keV for glass grains what can be well-compared with the point at which the measured equilibrium potential curve profile (Fig. 8) deviates from the profile equably decreasing at a higher beam energy range that would be expected for larger grains. Unfortunately, no data for another grain diameter are available at present. We would like to stress out here that only given assumptions are used for η computations, no further adjustment of any parameter need to be done. Note that the η enhancement for a spherical sample shape is $\approx 25\,\%$ and $\approx 200\,\%$ for gold and glass, respectively, and that the η curve maximum of glass is not as sharp as that for a planar sample what makes modelled glass η curves more appropriate for grains.

Although an energy spectrum of SEs is generally expected to be a Maxwellian-like, *Velyhan et al.* [2001] showed that the Draine Salpeter distribution [*Draine and Salpeter*, 1979] seems to be more suitable for metallic grains. Its profile has a narrower maximum comparing to the Maxwellian distribution and it differs mainly at a high-energy range having a significantly larger portion of hot electrons. Since the surface potential is given by the secondary emission yields and by the distribution of SEs, it is useful to plot the surface potential as a function of δ^* for both suggested distributions. We did it and found out that the rise of a surface potential with δ^* follows the same curve until $\delta^* \approx 1.5$ if the characteristic energies

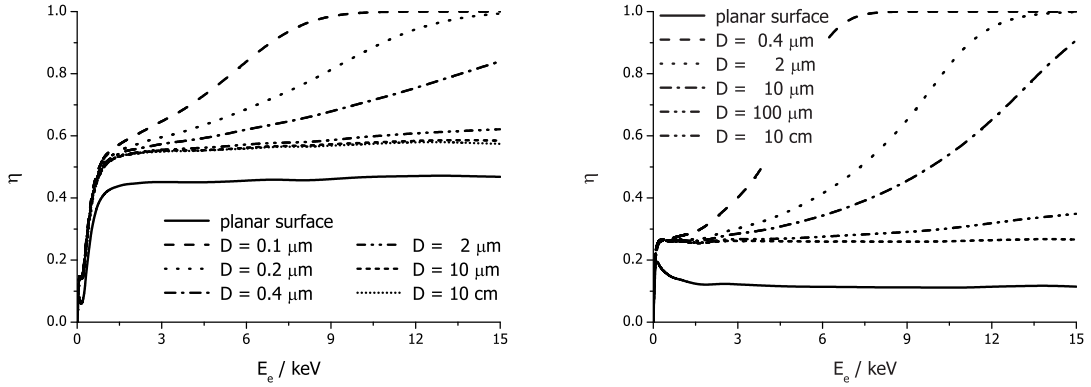

Figure 9. A modelled BE yield for samples of different sizes for glass (left) and gold (right). Whereas η enhancement at higher energies occurs for gold grains only at diameters smaller than ≈ 2 μm in a given energy range, it is appreciable until ≈ 100 μm diameters for glass grains.

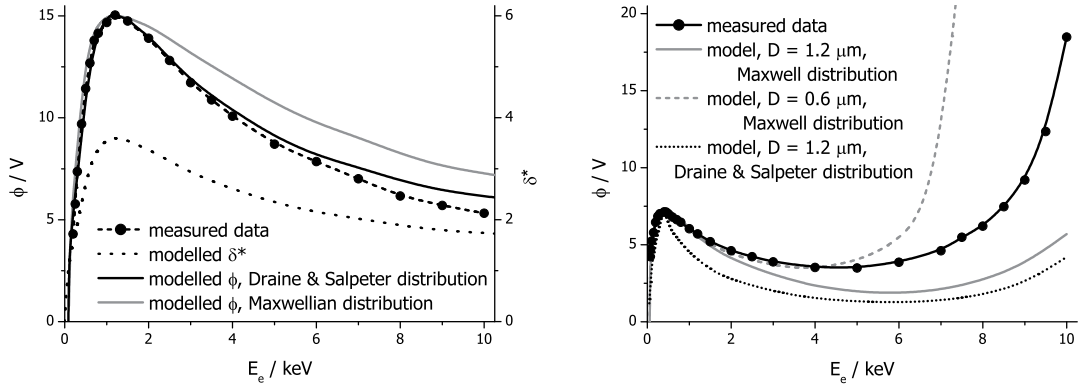

Figure 10. Comparison of measured data with our model for a 1.12 μm gold (left) and 1.2 μm glass (right) grains. Model parameters for gold are (using $\delta_{max} = 1.3$ and $E_{max} = 700$ eV for bulk): $\varepsilon = 31$ eV, $\Lambda = 1.25$ nm, $T_S = 3.1$ eV (first curve) and 4.3 eV (second curve). Model parameters for glass are (using $\delta_{max} = 2.3$ and $E_{max} = 300$ eV for bulk): $\varepsilon = 17$ eV, $\Lambda = 2.5$ nm, $T_S = 1.8$ eV (first two curves) and 1.2 eV (dotted curve).

(temperatures) of both distributions are equal. Above this value, the potential rises nearly linearly for the Draine Salpeter distribution, whereas the rise is much slower for the Maxwellian distribution.

The comparison of modelled and experimental data and determination of model parameters proceed in several steps. Since the maximum of ϕ should correspond to the maximum of δ^*, δ^* as a function of the beam energy has been computed for various Λ. Among them, that one peaking at the same energy as the measured $\phi(E_e)$ have been chosen and Λ was determined this way. From curves shown in Fig. 4 (left) can be found the corresponding product $\varepsilon\delta_{max}$. In order to established the characteristic energy loss, $\varepsilon\delta$ as a function of the beam energy for a planar sample has been computed using already determined value of Λ and its maximum was found. Since $\delta_{max} \approx 1.3$ for a planar sample [*Seiler*, 1983], ε could be obtained. After the above procedure, $\delta(E_e)$ is known and since $\eta(E_e)$ was already established, $\delta^*(E_e)$ is know as well. As a last step, both suggested distributions of SEs have been applied and ϕ curves for different temperatures of secondaries have been computed and those that exhibited the same maxima as the measured curve was chosen. The results are plotted in Fig. 10 together with $\delta^*(E_e)$ resulting from the model. It could be noted that the profile using the Draine Salpeter distribution matches experimental data better than the other. We would like to note that the Maxwellian distribution provides a much broader peak of the potential profile and thus, it differs from the data in a region where both model and experiment would be considered as most reliable.

A similar fitting procedure was done for the 1.2 μm glass grain. Modelled equilibrium surface potential curves using both energetic distributions of SEs are plotted in Fig. 10 (right). In this case, the measured potential profile near the first local maximum is a better approximation when the Maxwellian distribution is used. However, the second potential growth was determined at higher beam energies than was observed. A comparison to a smaller grain leads to estimation that a grain diameter near to two thirds of the real one would match the measurements. Nevertheless, a more precise incorporation of the glass structure into model assumptions or considering some admixtures in the glass grain would have the same effect, i.e., the second potential growth position would shift for a certain diameter. Note that the growth becomes very rapid above ≈ 10 V as only a few SEs may get such high energies.

Conclusion

The numerical and experimental investigations of the charging of dust grains illuminated by the electron beam have shown that the new version of the developed model describes very well all basic features of measured profiles of the electron yields for large planar samples as well as of the surface potential for small spherical grains. Consequently, we can conclude that the model includes principal processes leading to the emission of secondary electrons.

The best agreement of the model and experiment was achieved for metallic (Au in the investigated case) planar surfaces. The values of η are fully consistent with published data but the values of δ resulting from the model are a little larger than expected for higher beam energies. We suggest that this difference is caused by neglecting of the X-ray production in our model.

Yields of secondary emission from small grains cannot be measured directly and thus, we have

compared the measured and computed equilibrium surface potentials that depend also on the spectrum of secondary electrons. Using values of δ_{max} for the gold, we have found an excellent agreement of measured and modelled potential profiles under assumption that the secondary electron spectrum is of Draine Salpeter type. A similar conclusion can be found in *Velyhan et al.* [2001]. Small overestimation of the grain potential for high beam energies is probably connected with above mentioned neglecting of the X-ray production. On the other hand, the modelled potential profiles for glass grain suggest that the Maxwellian-like spectrum of secondary electrons should be expected for this material. Nevertheless, a further experimental investigation of these spectra is desirable. Values of all free model parameters (given in the caption of Fig. 10) were established in the excepted range for both grain materials.

We have found that smaller grains exhibit larger potentials (larger total secondary currents) in the investigated range of energies. This effect could lead to positive potentials of small grains, whereas larger grains would be charged negatively when immersed in a hot plasma. *Chow et al.* [2000] showed recently that this could be an explanation for a phase of rapid grain growth in the sheath edge of industrial plasma applications.

Whereas the low-energy part of the model curve describes well the values obtained on glass grains, the high-energy tail corresponds to the grain of a smaller diameter. A possible reason is that the Bethe stopping power equation can be used properly only for pure elements. A better approach would be to compute the stopping power for compounds from optical absorption data and we plan to do it in the future.

The presented approach to the modelling of the secondary emission from dust grains is very promising but new interactions should be taken into account in following development.

Acknowledgments. This work is a part of the research plan MSM 0021620834 that is financed by the Ministry of Education of the Czech Republic and was partly supported by the Czech Grant Agency under contract number 202/03/H162. The authors would like to thank also to Prof. Vítek for his inestimable help and endless discussions and to referees for their constructive comments and suggestions.

References

Bronstein, I. and Fraiman, B., *Secondary Electron Emission (in Russian)*, Nauka, Moskva, 1969.

Čermák, I., Pavlů, J., Žilavý, P., Němeček, Z., Šafránková, J., and Richterová, I., 3D Electrodynamic Quadrupole: A Nondestructive Analysis of Single Dust Grains, in *WDS'04 Proceedings of Contributed Papers: Part II — Physics of Plasmas and Ionized Media*, edited by J. Šafránková, pp. 279–286, Matfyzpress, 2004.

Chow, V., Mendis, D., and Rosenberg, M., Secondary emission from small dust grains at high electron energies, *IEEE Transactions on Plasma Science*, *22*, 179–186, 1994.

Chow, V. W., Mendis, D. A., and Rosenberg, M., Grain growth in processing plasmas, *Plasma Physics and Controlled Fusion*, *42*, 21–27, 2000.

Czyżewski, Z., O'Neill MacCallum, D., Romig, A., and Joy, D., Calculations of Mott scattering cross sections, *J. Appl. Phys.*, *68*, 3066–3072, 1990.

Draine, B. and Salpeter, E., On the Physics of Dust Grains in Hot Gas, *Astrophys. J.*, *231*, 77–94, 1979.

Egerton, R., *Electron Energy-Loss Spectroscopy in the Electron Microscope*, Plenum Press, New York, 1986.

Horányi, M., Charged Dust Dynamics in the Solar System, *Annu. Rev. Astron. Astrophys.*, *34*, 383–418, 1996.

Hovington, P., Drouin, D., and Gauvin, R., CASINO: A New Monte Carlo Code in C Language for Electron Beam Interaction — Parts I–III, *Scanning*, *19*, 1–35, 1997.

Joy, D., *Monte Carlo Modeling for Electron Microscopy and Microanalysis*, Oxford University Press, New York, 1995.

Kimura, H. and Mann, I., The Electric Charging of Interstellar Dust in the Solar System and Consequences for Its Dynamics, *Astrophys. J.*, *499*, 454–462, 1998.

Meyer-Vernet, N., Flip-flop of electric potential of dust grains in space, *Astron. Astrophys.*, *105*, 98–106, 1982.

Mott, N. and Massey, H., *Theory of atomic collisions*, Oxford University Press, New York, 1965.

Richterová, I., Němeček, Z., Šafránková, J., and Pavlů, J., A Model of Secondary Emission From Dust Grains and Its Comparison With an Experiment, *IEEE Trans. Plasma Sci.*, *32*, 617–622, 2004.

Seiler, H., Secondary electron emission in the scanning electron microscope, *J. Appl. Phys.*, *54*, R1–R18, 1983.

Sternglass, E., *On the Phenomenon of Secondary Electron Emission from Solids*, Master's thesis, Cornell University, 1951.

Švestka, J., Čermák, I., and Grün, E., Electric charging and electrostatic fragmentation of dust particles in laboratory, *Adv. Sp. Res.*, *13*, 199–202, 1993.

Velyhan, A., Němeček, Z., and Šafránková, J., Secondary electron emisson from small metallic grains, in *WDS'01 Proceedings of Contributed Papers: Part II — Physics of Plasmas and Ionized Media*, edited by J. Šafránková, pp. 267–272, Matfyzpress, 2001.

Verma, R., The backscattering electrons from reduced lead glass, *J. Phys. D: Appl. Phys.*, *10*, 1735–1739, 1977.

Whipple, E. C., Potentials of surfaces in space, *Reports of Progress in Physics*, *44*, 1197–1250, 1981.

Ziemann, P., Liu, P., Kittelson, D., and McMurry, P., Electron Impact Charging Properties of Size-Selected, Submicrometer Organic Particles, *J. Phys. Chem.*, *99*, 5126–5138, 1995.